Lateral ultrasound strain imaging using subband processing

Hui Peng[a], and Juhong Tie

School of Software Engineering, Chengdu University of Information Technology, Chengdu, China

Abstract. Since most biological tissues are nearly incompressible, the axial compression leads to expansion in the lateral and elevational directions. Although axial strain is the main component of three dimensional strain field, estimation of the lateral strain may provide important additional information on the tissue mechanical properties. In this paper, we employed the idea and principle of image compounding and proposed a subband processing method to estimate lateral strain. To keep lateral radio freqency (RF) signal bandwidth and strain resolution, we split axial RF signal into several subband signals and then estimate lateral strains of these subband signals along lateral direction, finally average these strains to get a lateral compounded strain image. The simulation results demonstrate that the elastographic signal-to-noise ratio of the lateral compounded strain image is improved by 48% using this subband processing method, compared with the conventional method.

1 Introduction

Ultrasound strain imaging is a new medical imaging modality that can provide relative stiffness information of biological tissue for clinician to diagnose deceases such as tumors or cancers. However, poor quality of strain imaging may degrade its clinical value [1]. Therefore, improving the quality of strain image is an important and meaningful research direction [2-5].

For ultrasound B-mode imaging, spatial compound method is used to reduce speckle noise. Several different angular B-mode images from same scanning tissue region are averaged to produce one compounded B-mode image which SNR can be improved by $\sqrt{N}$ times [6]. Reference [4] first applied spatial compound method to strain imaging. Reference [5] proposed a transmit-side frequency compound method in which several sub transmit-side frequency strain images are averaged to produce a compounded strain image to reduce elastography nosie. We first proposed a subband processing method to estimate axial strains [3].

Since most biological tissues are nearly incompressible, the axial compression leads to expansion in the lateral and elevational directions [7]. Although axial strain is the main component of three dimensional strain field, estimation of the lateral displacement and strain may provide important additional information on the tissue mechanical properties. By taking advantage of the lateral estimation technique, shear strains and the Poisson's ratio have been shown capable of being estimated [8]. In this paper, we employed the idea and principle of image compounding and proposed a subband processing method to estimate lateral strain. We also tested this method in simulations.

[a] Corresponding author: penghui@cuit.edu.cn

2 Method

2.1 Strain image compounding theory

The correlation of two sub-elastograms P and Q, with the size of m*n pixels can be evaluated by the normalized correlation coefficient, p, 0<=p<=1 [5]:

$$\rho = \frac{\sum_{i=1}^{m}\sum_{j=1}^{n}(P_{i,j}-\bar{P})(Q_{i,j}-\bar{Q})}{\sqrt{\sum_{i=1}^{m}\sum_{j=1}^{n}(P_{i,j}-\bar{P})^2\sum_{i=1}^{m}\sum_{j=1}^{n}(Q_{i,j}-\bar{Q})^2}} \tag{1}$$

where $P_{i,j}$ and $Q_{i,j}$ are strains at location (i, j), $\bar{P}$ and $\bar{Q}$ are mean strains for P and Q respectively

The quality of strain image is usually evaluated by elastographic signal-to-noise ratio (SNRe) as:

$$\mathrm{SNRe} = \frac{\mu}{\sigma} \tag{2}$$

where μ and σ are, respectively, the mean and standard deviation of the strain estimates in region of uniform elasticity.

Define the random variables Xi(i=1,2,...,N, N>=2) of N sub-elastograms. The compounded elastogram, $\bar{X}$, is obtained by averaging N sub-elastograms. The SNRe of the compounded elastogram will be [5]:

$$\mathrm{SNRe}' = \frac{E(\bar{X})}{\sqrt{Var(\bar{X})}} = \frac{\mu}{\sigma}\sqrt{\frac{N}{1+(N-1)\rho}} \tag{3}$$

where $E(\bar{X})$ and $Var(\bar{X})$ denote the expectation and the variance of the compounded elastogram respectively. Therefore, from eqn. (3) we know the SNRe of the compounded elastogram will be increased by a factor of $a=\sqrt{N/(1+(N-1)\rho)}$ which has a maximum of $a=\sqrt{N}$ when all sub elastograms are completed decorrelated (i.e. p=0).

2.2 Subband processing

To achieve high axial strain resolution, some short pulses, such as two circle of sine wave, are sent into tissue. So, the echo radio frequency signal is usually broadband signal. The idea of subband processing is that a broadband signal is divided into many narrowband signals and these narrow band signals should cover whole frequency band to exploit all energy of the broadband signal [9-10]. To keep lateral RF signal bandwidth and strain resolution, we split axial RF signal into several subband signals and then estimate lateral strains of these subband signals along lateral direction, finally average these strains to get a compounded strain image. Bandwidth is important to strain imaging, because SNRe decreases with bandwidth according Cramer–Rao lower bound theory which states that the best achievable displacement variance is related to the center frequency, band width, correlation coefficient, window length and eSNR [11]. There are many subband methods. We adopt bandpass filter method to split axial RF signal to several subband signal. This method is shown in eqn. (4).

$$x_p(t) = BPF\{r(t),\ f_{p1}, f_{p2}\} \tag{4}$$

where r(t) is axial RF signal; f_{p1} and f_{p2} are the starting and ending frequency of pth subband respectively; $x_p(t)$ is pth subband RF signal; BPF{} denotes a function of bandpass filter. The center frequency of the pth subband is $f_p = (f_{p1}+f_{p2})/2$. For a axial RF signal of center frequency 5MHz, we split it into three subband signals which center frequencies are 3MHz, 5MHz and 7MHz respectively.

2.3 Estimation of lateral sub strain image

Each subband signal will be estimated to get its sub lateral strain image after Rf signal was devided into three subband signals. A strain image can be produced by displaying spatial derivatives from the displacement field. So, the key step of strain estimator is to estimate displacement of every correlation window according pre- and post deformation RF signals. There are many strain estimate methods such as cross-correlation, phase zero method, for producing axial strain image. Since lateral RF signal has more decorrelation noise inducing from axial displacements, some displacement estimate methods are not fit to estimate lateral displacement. We adopt phase zero method expressed in equation (5) to estimate sub lateral displacements [12].

$$\hat{d}_{k+1,n} = \hat{d}_{k,n} + \frac{\arg(\exp(-jw_0\hat{d}_{k,n})\sum_{t=n\Delta t}^{n\Delta t+T} x_{1b}^{*}(t)x_{2b}(t-\hat{d}_{k,n}))}{w_c} \tag{5}$$

where w_0 is the center frequency of sub lateral RF signal; w_c is the local frequency centroid; $\triangle t$ is the window spacing, T is the window length, $n\triangle t$ is the position of the start of the nth window. x_{1b} (t) and x_{2b} (t) are the baseband analytic signals of the sub lateral RF signals; $\hat{d}_{k,n}$ is the displacement estimate of the nth window at the kth iteration. At the first window, the search is initialized with $\hat{d}_{0,0}=0$. Subsequent searches are each initialized with the final displacement estimate from the previous window, i.e., $\hat{d}_{0,n}=\hat{d}_{K,n-1}$. We utilize the amplitude modulation correction method to correct amplitude modulation noise [13].

2.4 Lateral RF signal interpolation method

Since most clinical systems are using low-cost transducers with a small number of channels, the sampling rate of RF signal in lateral direction is greatly lower than that of axial RF signal. For a linear array transducer, the lateral sampling rate is determined by the number of scanning lines, and the axial sampling rate is determined by the axial sampling frequency. To achieve high accurate displacement estimates, the axial sampling frequency is generally at least 40MHz, so the sampling spacing in axial direction is generally at most 0.0385mm (supposed the sound speed is 1540m/s). For a 4 cm width of transducer with 192 channels, the sampling spacing in lateral direction is 0.208mm. So the sampling rate in lateral direction is lower five times than that in axial direction. Low sampling rate in lateral direction will reduce the accuracy of lateral displacement estimates [8]. If lateral sampling frequency satisfies the Nyquist sampling theorem, the lateral signal can be interpolated to improve the accuracy of lateral displacement estimation. If the pitch of a linear array transducer is smaller than half beamwidth (as expressed in formula (6)), the lateral sampling frequency satisfies the Nyquist sampling theorem. Many interpolation methods like linear interpolation and cubic spline interplolation, etc. can be used in lateral RF signal. In this paper, we use cubic spline interplolation method, because cubic spline interplolation can increases the correlation coefficient compared with linear interpolation [8]. The interpolation coefficient is 1:10.

$$PITCH \le \frac{BW}{2} = \frac{2F\lambda}{2} = F\lambda \tag{6}$$

where BW is beamwidth; F is F-number of tranducer; λ is the wavelength of the emitted pulse.

3 Simulation method and results

3.1 Simulation method

The simulated RF data is obtained by the convolution of 2D PSF and tissue scatters.

$$r(x,z) = p(x,z) * s(x,z) + n(x,z) \tag{7}$$

where r(x,z) is the 2D RF signal ; x and z are the lateral and axial coordinates respectively; p(x,z) is the psf which is a Gaussian modulated sine function; s(x,z) is the scatters function; n(x,z) is white noise function. Scatterers are deformed by moving the location of the scatterers in the lateral direction using the analytic results of a simplified model developed in reference [14]. While both lateral and axial displacement is calculated in reference [14], we are only concerned with lateral displacement. The lateral displacement u(x,z) is:

$$u(x,z) = \frac{x}{r}\left(\frac{x^2}{r^2}Q(r) + \frac{z^2}{r}\frac{\partial Q(r)}{\partial r}\right) \tag{8}$$

and Q(r) is defined as:

$$Q(r) = \begin{cases} P\dfrac{2}{1+K}r & r \le R \\ P\left[1+\dfrac{1-K}{1+K}\left(2\dfrac{R^2}{r^2}-\dfrac{R^4}{r^4}\right)\right]r & r > R \end{cases} \tag{9}$$

where r is the distance between a sample volume and the center of the coordinate system, and $r^2 = x^2 + z^2$;P is a deformation scalar related to the magnitude of the applied force; R is the radius of the hard inclusion centered in the medium; K is the ratio of the young's modulus of the hard inclusion to that of the background soft medium; In this paper, we choose P=0.01, K=10,R=5mm.

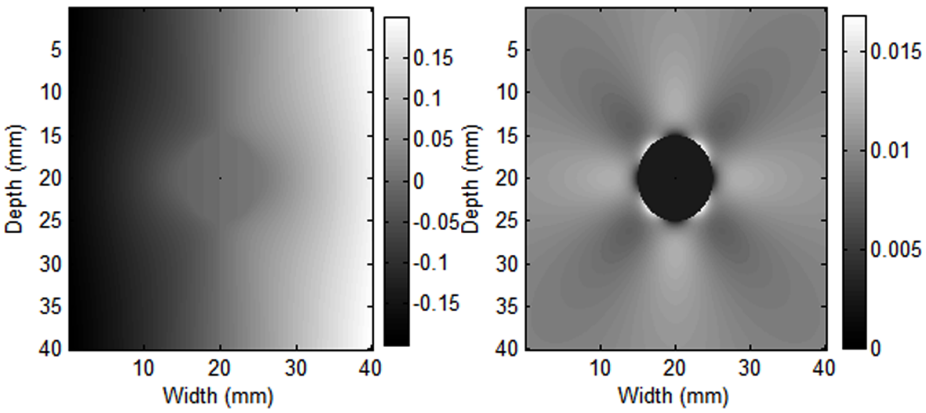

(a) Lateral displacements (b) Lateral strains

Figure.1 Lateral displacement and strain of scatter model

The center frequency of the conventional short pulse is 5MHz. The center frequencies of three subband signals are 3MHz, 5MHz and 7MHz respectively.

3.2 Simulation results

We compared the performance of subband method and conventional method in terms of SNRe and CNRe. For a pair of pre- and post-compressed RF fame, we use subband method and conventional method on them respectively to get the lateral strain image. Fig. 2 shows the results. Fig.2a shows lateral strain image using conventional method in which SNRe of background is 3.67 and SNRe of lesion is 3.77. Fig.2b , Fig.2c and Fig.2d show the lateral strain images using 3MHz,5MHz and 7MHz subband respectively. Fig.2e shows the compounded lateral strain image in which SNRe of background is 5.43 and SNRe of lesion is 5.90. Therefore, Compared with the conventional method, SNRe of background, SNRe of lesion and CNRe are increased by 48%, 56% and 120% respectively, using subband processing.

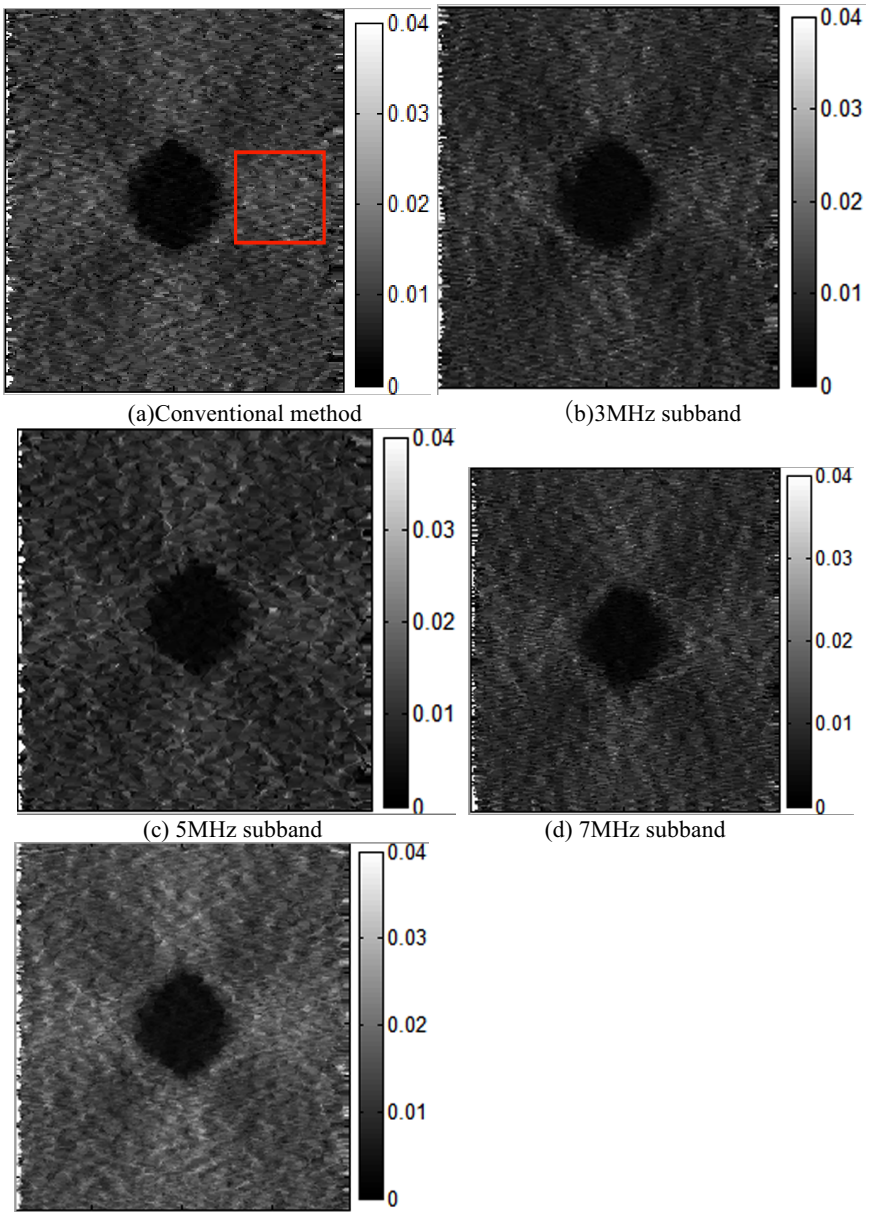

Fig.2 Comparision of conventional method and subband method. (a)Strain image using conventional method, SNRe of background is 3.67, SNRe of lesion is 3.77, CNRe is 4.33;(b)Strain image for 3MHz subband, SNRe of background is 3.69, SNRe of lesion is 4.09, CNRe is 14.55; (c) Strain image for 5MHz subband, SNRe of background is 3.56, SNRe of lesion is 3.96, CNRe is 13.59; (d) Strain image for7MHz subband, SNRe of background is 3.59, SNRe of lesion is 3.59, CNRe is 13.77; (e)Compounded strain image, SNRe of background 5.43, SNRe of lesion is 5.90, CNRe is 31.57.

Table 1 correlation coefficients of three subband images

	3MHz subband	5MHz subband	7MHz subband
3MHz subband	1.0	0.0165	0.0096
5MHz subband	0.0165	1.0	0.1096
7MHz subband	0.0096	0.1096	1.0

4 Discussion and conclusion

SNRe gain and CNRe gain by using subband processing can be explained from strain image compounding theory. The correlation coefficients between three sub strain images are listed in table 1 in which the average correlation coefficient is 0.045. The SNRe of the compounded strain image which is averaged by three sub strain images can be improved by $\sqrt{3/(1+2\rho)}-1$ times, according to strain image compounding theory. Therefore, the SNRe of the compounded strain image in Fig.2e should be improved by 66% in theory. The SNRe gain of the lesion of the compounded strain image in Fig.2e is 57% which is close to the theoretical value. Although the SNRe gain of the background of the compounded strain image in Fig.2 e is 48%, it differs from the theoretical value 18%. This is because the strain field of the whole background is not uniform, and the variances of three sub strain images are not quit identical, which will result in certain deviation from the theoretical value of the SNRe of the compounded strain image. It can be seen from in Fig.2 that the SNRes of three sub strain images are nearly same with that of the stain imaing using conventional method. This result indirectly shows that the subband splitting of RF signal along the axial direction does not result in the decrease of the bandwidth of the lateral RF signal, which is the reason why we splitted the RF signals into three subbands along the axial direction. In conclusion, the quality of lateral strain image can be improved significantly using subband processing.

Acknowledgments

This work is in part supported by the Scientific Research Foundation of CUIT (Project No. KYTZ201320), and also in part supported by the Scientific Research Foundation of Education Department of Sichuan Province (Grant No. 14ZB0185).

References

1. K.M. Hiltawsky,M. Kruger, C. Starke, et al. Ultrasound Med. Biol., **27**, 1461(2001)
2. H. Peng, D. C. Liu, Biomed. Signal Process. Contr., **8**,130(2013)
3. H. Peng, D.C. Liu, J. Sichuan Univ. (Eng. Sci. Ed.), **44**, 127(2012)
4. M. Tanter,J. Bercoff, L. Sandrin,M. Fink, IEEE Trans. Ultrason., Ferroelect., Freq. Contr., **49**,1363(2002)
5. S. Cui, D.C. Liu, IEEE Trans. Ultrason., Ferroelect., Freq. Contr., **58**,509(2011)
6. H. Ping, Ultrason Imag., **19**, 251(1997)
7. E. Konofagou, and J. Ophir,Ultrasound in Med. & Biol., **24**, 1183(1998)
8. J. Luo, and E.E. Konofagou,Ultrasound Med Biol., **35**, 1352(2009)
9. F. Gran, J. Udesen, M. B. Nielsen, J.A. Jensen, IEEE Trans. Ultrason., Ferroelect., Freq. Contr., **55**, 2211(2008)
10. J. Udesen,F.Gran, M. B. Nielsen, J.A. Jensen, Procedings of the IEEE Ultrasonics Symposium, 2006
11. W.F. Walker, G.E. Trahey, IEEE Trans. Ultrason., Ferroelect., Freq. Contr., **42**, 301(1995)

12. A. Pesavento, C. Perrey, M. Krueger, H. Ermert, IEEE Trans. Ultrason., Ferroelect., Freq. Contr., **46**, 1057(1999)
13. J. E. Lindop, G. M. Treece, A. H. Gee, R. W. Prager, IEEE Trans. Ultrason., Ferroelect., Freq. Contr., **54**, 1751(2007)
14. L. Huang, Y. Petrank, S.W. Huang, C. Jia and M. O'Donnell, IEEE Trans. Ultrason., Ferroelect., Freq. Contr., **56**,1368(2009)